5-1-2018

Virtual Structural Analysis of Bone Fracture Healing from Low-Dose Clinical CT Scans

Peter Schwarzenberg
Lehigh University, pschwarzenberg1@gmail.com

VIRTUAL STRUCTURAL ANALYSIS OF BONE FRACTURE HEALING FROM LOW-DOSE CLINICAL CT SCANS

by

Peter Schwarzenberg

A Thesis

Presented to the Graduate Research Committee

Of Lehigh University

In Candidacy for the Degree of

Master of Science

in

Mechanical Engineering

Lehigh University

May 2018

Certificate of Approval

This thesis is accepted and approved in partial fulfillment of the requirements for the Master of Science.

_____
Date

_____
Thesis Advisor, Dr. Hannah Dailey

_____
Chairperson of Department, Dr. Gary Harlow

Table of Contents

List of Tables:

List of Figures:

Abstract

Bone fractures often heal by forming a soft external bridge called a *callus*, which gradually hardens over time and restores the structural stiffness of the bone. In clinical studies focused on bone healing, healing progress is usually tracked using subjective assessments such as pain and mobility scores, qualitative observations of callus on X-rays, and incidence of complications such as implant fatigue failure. This data can be highly variable, leading to study designs that require very large multi-center trials with thousands of cases to detect differences between groups.

Accordingly, the purpose of this thesis is to propose a new technique for assessing bone healing using virtual mechano-structural analysis of computed tomography (CT) scan data. In this work, CT scans from 19 fractured human tibiae (shinbones) at 12 weeks after surgery were segmented and prepared for finite element analysis (FEA). Boundary conditions were applied to the models to simulate a torsion test that is commonly used to assess the structural integrity of long bones in animal models of fracture healing. The output of each model was the virtual torsional rigidity (VTR) of the healing zone, normalized to the torsional rigidity of that same patient's virtually reconstructed tibia. This provided a structural measure to track the percentage of healing each patient had undergone. Callus morphometric measurements were also collected from the CT scans.

Results from this study showed that morphometric data such as callus volume and density had weak non-significant correlations to a patient's healing. However, VTR had a strong correlation of $R^2 = 0.699$ ($p < 0.0001$) with the reconstructed VTR. Furthermore, more than 75% of patients achieved a normalized VTR (torsional rigidity relative to

uninjured bone) of 75% or above. This finding suggests that a new clinically relevant guideline – the "75/75" rule – may be useful for benchmarking expectations for normal healing. Under this rule, surgeons should expect 75% of tibial fracture patients to achieve at least 75% of their own intact rigidity at 12 weeks post-op.

In summary, this study is the first-ever application of image-based structural analysis to clinical (human) CT scan data for assessment of bone healing. The methods proposed may provide the foundation for a new paradigm of robust and statistically powerful clinical research in orthopaedic trauma.

I. Introduction

Fractures of the long bones (e.g. tibia/shinbone, femur/thighbone) typically heal by a process known as secondary fracture healing. Shortly after the injury, a cartilaginous bridging structure called a *callus* forms across the fracture gap (see Figure 1). Over a period of weeks or months, the callus grows and gradually ossifies (hardens by forming calcified new bone) to restore the structural stiffness of the bone. Normally, a fracture of the lower extremity heals in about four to five months [1], but occasionally this process may become delayed or stalled, resulting in a clinical condition known as non-union.

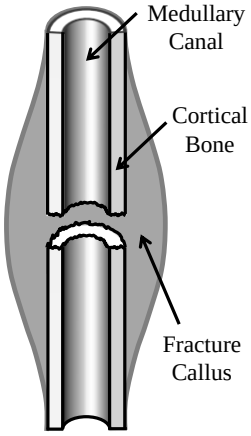

Figure 1: Schematic of a long-bone fracture healing by formation of an external bridging callus.

In clinical studies focused on assessment of bone healing, healing progress is usually tracked using subjective assessments such as pain and mobility scores, clinical assessments of X-rays, and recorded complications such as non-unions, implant fatigue failures, and reoperations. These research designs are significantly limited by the variability of the data produced and lack of statistical power. For example, in one large device-related trial pertaining to angular-stable fixation of distal tibia fractures, patients reported pain levels at rest and during weight bearing, but the highly variable data showed a strong trend toward decreasing pain over time without a detectable difference in pain between the groups based on fixator type [2]. When studies focus on relatively rare complications, such as nonunion or reoperation, very large multi-center trials with

thousands of cases are needed to detect differences between groups, such as in the SPRINT study on reamed versus un-reamed tibial nailing [3].

Focusing on radiographic assessment, lack of consistency in the evaluation of fracture healing has been a widely recognized clinical problem in orthopaedic trauma [4] and the need for greater objectivity led to the development of the radiographic union scale for tibial fractures (RUST). The RUST X-ray scoring system systematically rates the visible fracture callus at each of the four cortices on a scale from no callus present (1 point) to fully bridged (3 points), with the sum of these scores indicating the progress of healing (see Table 1) [5].

Table 1: RUST score assessment of fracture healing from clinical X-rays.

Score per Cortex	Callus	Fracture Line
1	Absent	Visible
2	Present	Visible
3	Present	Invisible

For the representative case shown in Figure 2, the attending orthopaedic surgeon assigned a RUST score of 12, indicating callus present and fracture line invisible at all four cortices (anterior, posterior, medial, and lateral). The RUST approach has demonstrable intra- and inter-observer reliability [5], [6], has been adapted for use in metaphyseal fractures [7], and has become a commonly used tool in the design of randomized controlled trials [8]. The advantage of RUST scoring is that it was designed to capture the structural development of external callus at the fracture site and has demonstrated utility as a tool to differentiate between united and nonunion fractures (RUST > 10 for union) in clinical studies [9]–[11]. However, within a cohort of normally progressing fractures, within-group variability can

be high, especially at early time points, and the RUST score is lacking in sensitivity to detect subtle changes in callus mechanical integrity, leading to a need for large patient recruitment targets.

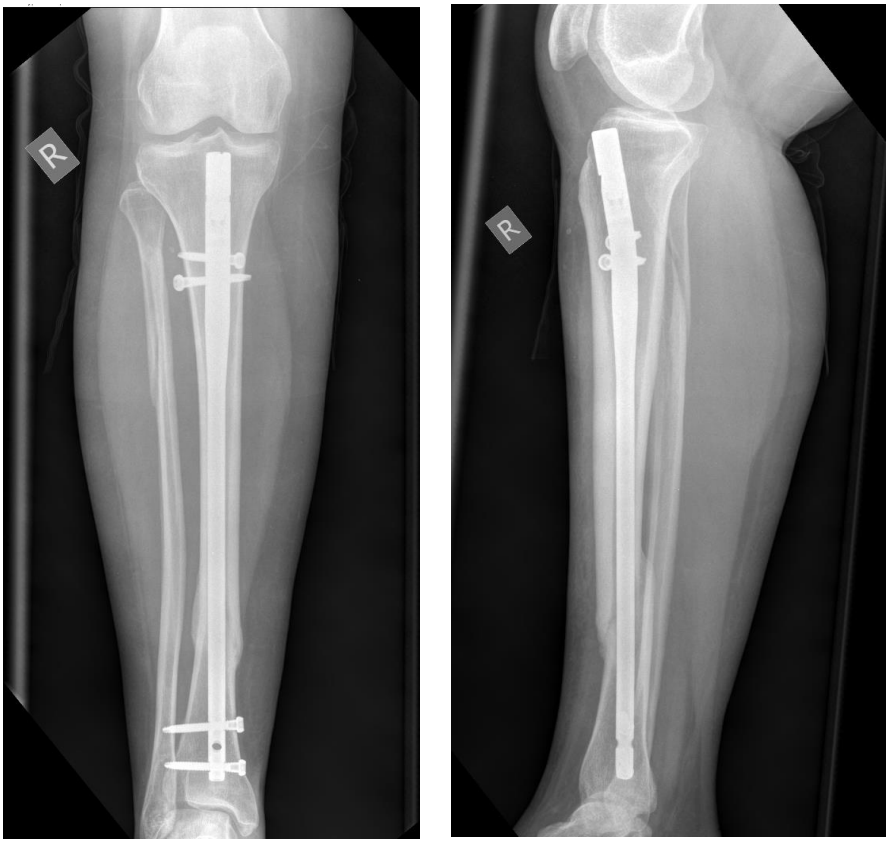

Figure 2: Pair of X-rays (anteroposterior and lateral views) for a tibial fracture from this case series at 12 weeks post-injury. These images correspond to the same individual shown in Figures 3 and 4.

In contrast to the current limitations of clinical research design, preclinical studies have demonstrated the power of 3-D imaging to assess not just callus presence and connectivity, but also the material properties and complex geometry that together define the objective structural integrity of the callus region. Methods developed for ovine (sheep) models have been shown to successfully monitor the *in vivo* bone adaptive response within an individual animal *in silico* utilizing computed tomography (CT) scan data [12]. CT

scans, sometimes known as *CAT scans*, produce cross-sectional images by sequentially exposing an object or body part to X-rays at different angles. This data can then be reconstructed into 3D visualizations using computerized image analysis methods.

The published history of CT-based analysis of fracture healing includes simplistic structural studies that idealized the fracture as basic geometric shapes to approximately calculate strength [13]. Additionally, methods have been developed to assign element-wise material properties for finite element (FE) models [14]–[16]. However, these studies have not been conducted in humans and recent technological advances in image analysis and expanding capabilities for very large computational simulations indicate that more detailed analysis may now be possible. Human studies have employed computational analysis techniques, but are not structural and many are limited to 2D plain film X-ray analysis [17]. Furthermore, published modeling techniques based on post-mortem high-resolution micro-CT scans are not translatable to clinical research designs for obvious reasons. Accordingly, the purpose of this study was to develop a robust method for carrying out structural evaluations of fracture healing using low-dose CT scans taken of clinical fractures treated by routine surgical fracture fixation.

II. Methods

A. Clinical Study Information

A sequential cohort of N = 19 tibial fracture patients was prospectively recruited from Cork University Hospital, a Level I trauma centre located in Cork, Ireland. The primary inclusion criteria were diaphyseal or proximal/distal extra-articular tibial fractures (AO/OTA 41-A2/A3, 42-A, 42-B, 42-C, and 43A) in patients 18 years of age or older and deemed clinically suitable for reamed intramedullary nail fixation. All patients provided written informed consent. Exclusion criteria included but were not limited to chronic disease, osteoporosis, pregnancy, polytrauma, deformity or previous metalwork. All tibial nails were statically interlocked with two proximal and two distal screws. Patient and injury characteristics are shown in Table 2. For each case, the injury severity is characterized as closed (no breakage of the skin) or open (any skin injury, ranging from minimal to severe, also known as a "compound" fracture). The OTA/AO classification is also given as a reference to the system of morphological characterization used by surgeons to describe fractures. In this system, "42" refers to the location (tibia shaft fracture), the letter refers to the general shape (A – simple, B – wedge, C – complex) and the number refers to the sub-type. Renderings of each fracture in this series can be found in Figures 4-7. RUST scores for each patient were independently assessed by the attending orthopaedic surgeon using standard X-rays taken at 12 weeks and this data was blinded until completion of the CT-based structural analysis.

Table 2: Patient data of the 19 individuals included in this study who completed CT scanning at 12 weeks post-op

CT Case Number [-]	Gender [Male/Female]	Age [Years]	Injury [Closed/Open]	OTA/AO [-]
CT01	Female	51	Closed	42A2
CT02	Male	52	Closed	42A1
CT03	Male	32	Open	42B3
CT04	Male	32	Closed	42A3
CT05	Male	55	Closed	42A1
CT06	Male	58	Closed	42A3
CT07	Male	33	Closed	42A2
CT08	Female	39	Open	42B2
CT09	Male	65	Closed	42C2
CT10	Male	33	Closed	42A3
CT11	Male	20	Closed	42A3
CT12	Male	45	Open	42A2
CT13	Male	50	Closed	42A1
CT14	Male	24	Closed	42A1
CT15	Male	39	Closed	42A2
CT16	Male	29	Closed	42A3
CT17	Male	57	Closed	42B3
CT18	Male	53	Closed	42A1
CT19	Male	18	Closed	42A3

B. CT Scan Protocol

Low-dose CT scans were performed 12 weeks after surgery. CT scans were performed on a GE (General Electric Healthcare; WI, USA) Discovery CT750 HD with X-ray tube voltage of 80kV, current-time product of 10mAs, gantry rotation speed of 0.4 seconds, and a pitch of 0.51. GE's VEO Model-Based Iterative Reconstruction (MBIR) algorithm was used with a resolution improvement, RP05, filter kernel [19], [20]. The resulting scan resolution had a slice thickness of 0.625 mm and final voxel size of $0.625 \times 0.488 \times 0.488$ mm^3 (Figure 3a).

C. Scan Processing and Injured Limb Reconstruction

Anonymized CT scan image sets were transferred from the hospital in DICOM file format and processed using the Mimics Innovation Suite (Materialise, Leuven, Belgium). The segmentation workflow (Figure 3) in Mimics allows creation of optimized 3D surface models by applying density-based threshold rules to the CT scan images and thereby selecting cohesive regions of voxels that represent different tissues (Figure 3b). For this study, threshold values of 400-1400 Hounsfield Units (HU) were chosen to segment the callus and values of 1400-2700 HU were chosen to segment cortical bone. The lower bound was chosen by first applying a 50/50 mixing rule of woven bone and cartilage as a baseline assumption [21]. This threshold was then increased until the surrounding soft tissue was no longer being captured for several representative scans. The resulting 400 HU threshold was then uniformly applied for all models. For the upper bound, the threshold was increased to capture as much existing cortical bone as possible without capturing any voxels from the high-density intramedullary nail. Lastly, the division between existing cortical bone and new callus was chosen by applying a range to several representative scans and visually inspecting for any non-physical features at the fracture site, resulting in the threshold bounds stated above.

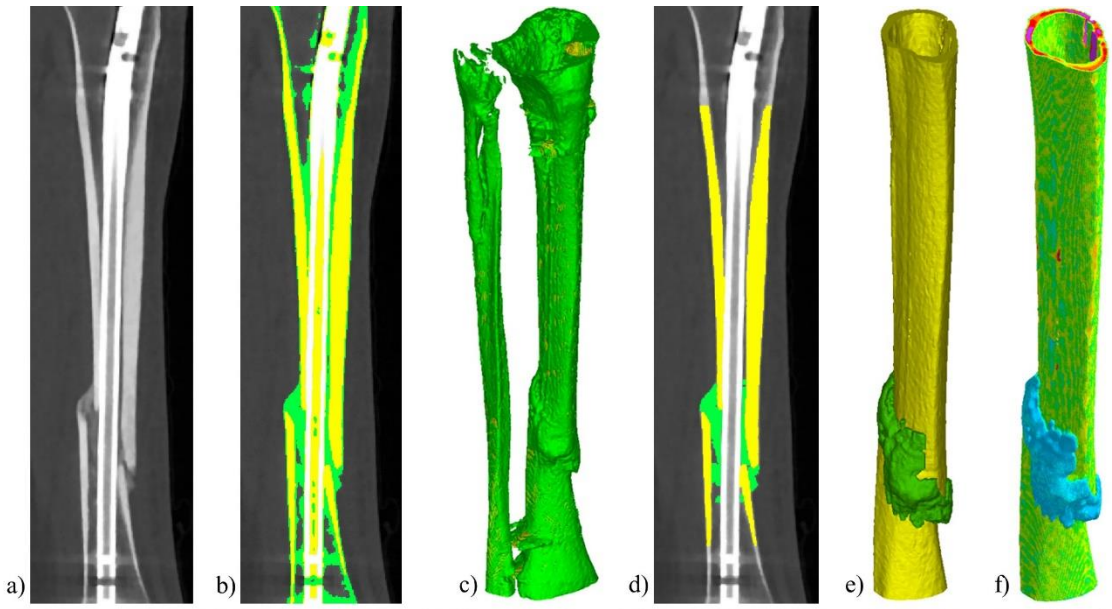

Figure 3: (a) Sagittal slice view of CT DICOM stack without masks applied. (b) Sagittal view with bone (yellow 1400-2700 HU) and callus (green 400-1400 HU) thresholds applied. (c) 3D surface model before morphometric region growing and erosion and dilation tools applied. (d) Sagittal slice view with bone and callus thresholds after morphometric tools applied. (e) 3D surface model after morphometric tools applied. This model is discretized and meshed to create a finite element mesh. (f) Elastic modulus contour plot of finite element assignment.

A parameter sensitivity study investigated the influence each threshold parameter has on intermediate outcome measurements. A ± 100 HU variation in the upper threshold value had a percent volume change of less than 2% on the existing cortical bone segmented. Varying the middle threshold by ± 100 HU resulted in a percent change in volume of less than 6% in the callus region and less than 4% in the existing cortical bone. While the variation of the middle threshold value may change the morphometric parameters, the final unified structural model remains the same. Lastly, a lower threshold variation of ± 100 HU had a percent change in volume of less than 20% on the callus region. The lower threshold has the most potential to be problematic because the tissue density becomes comparable to

that of the soft tissue envelope and can produce obvious non-physical segmented callus volumes. Even though the sensitivity is high, the rationale for the set point is based on choosing a minimum that produces a clinically relevant structure.

In preparation for volumetric discretization, a series of surface cleanup operations were performed to optimize the outer envelope of each segmented region. Region growing and morphometric erosion and dilation tools were used to refine the segmented cortical bone and callus regions from each scan (Figure 3d). After cleanup, these regions were unified into a single structural body. Cut surfaces were created at the proximal and distal ends, just distal to the proximal screws and just proximal to the distal screws, in preparation for finite element (FE) boundary condition (BC) application. The final unified surface was smoothed to remove artifacts from the scanning process and improve meshability. To quantify the effect of smoothing on the final model geometry, we conducted a smoothing sensitivity study showing that smoothing produced less than a 0.25% volume changes on all models.

D. Finite Element Model Creation

Meshing for FE structural mechanics was carried out using a dedicated toolkit in Mimics. First, a triangular surface mesh was created on the unified surface body, and then volumetric discretization was completed using tetrahedral-4 elements. Since no additional information can be obtained under the resolution of the scan, the maximum edge length was set at 0.4 mm to be less than the original CT scan voxel size of $0.48 \times 0.48 \times 0.625$ mm^3. Element-wise mechanical properties were interpolated from voxel image intensities

using a previously published elastic modulus scaling law based on local Hounsfield units of the original CT scan: $E = 0.00704 \times HU$ GPa [22]. Patient model CT01 can be seen in Figure 4 along with a histogram of the elemental distribution. All patient models can be seen in Figures 5-7.

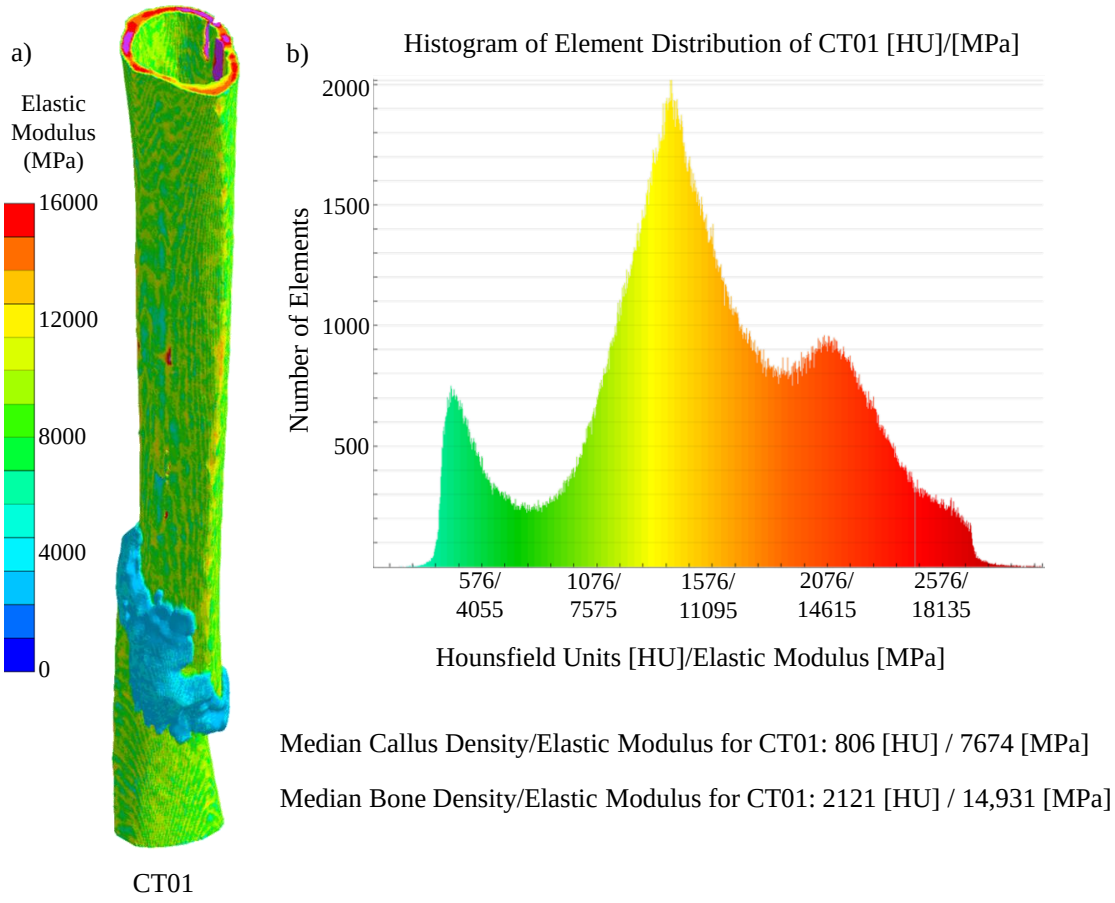

Figure 4: (a) Elastic modulus contour plot of finite element model CT01. Data corresponds to table 1 and 2. (b) Histogram of element distribution across CT01 of density/elastic modulus.

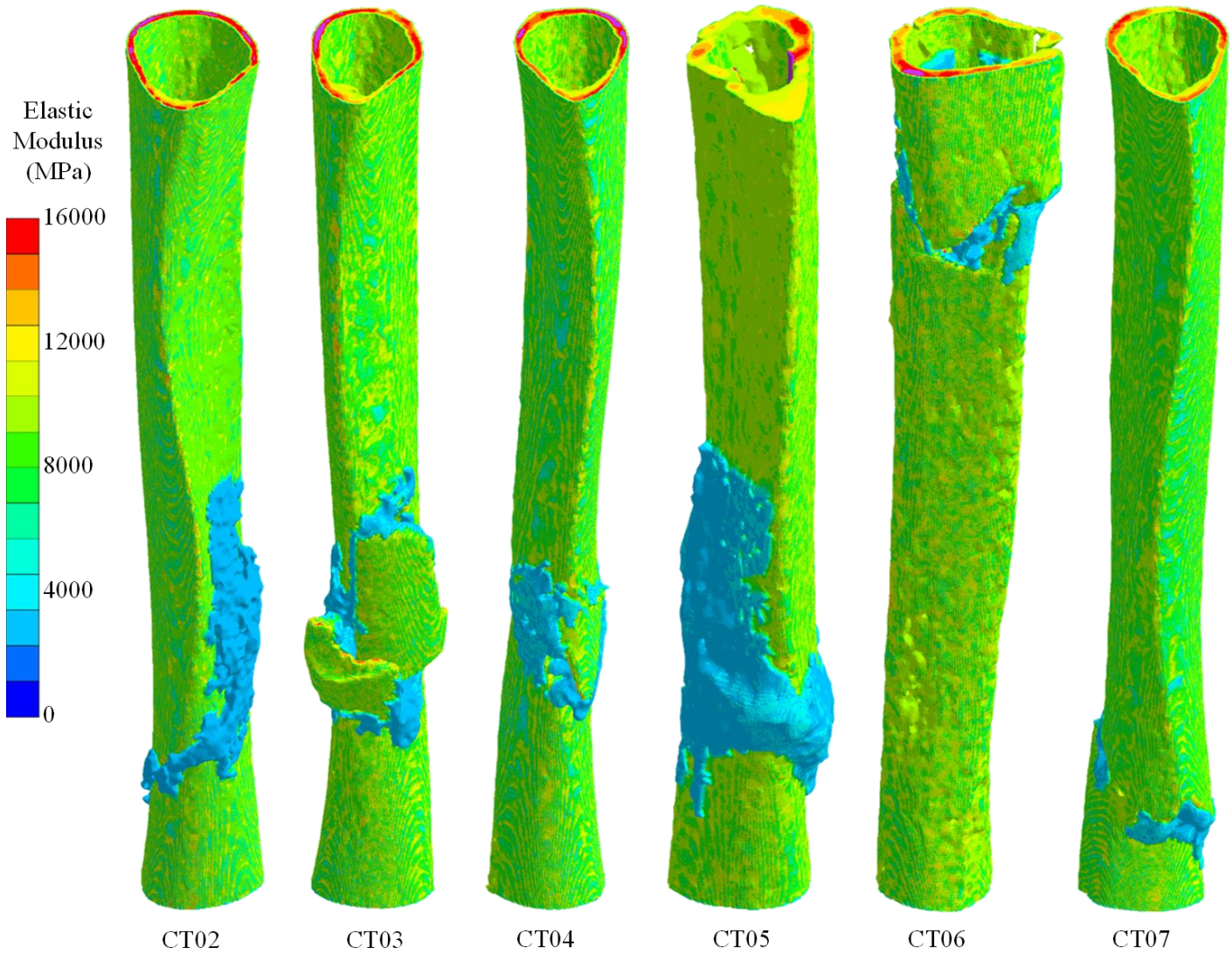

Figure 5: Elastic Moduli Contour Plots for CT02-CT07

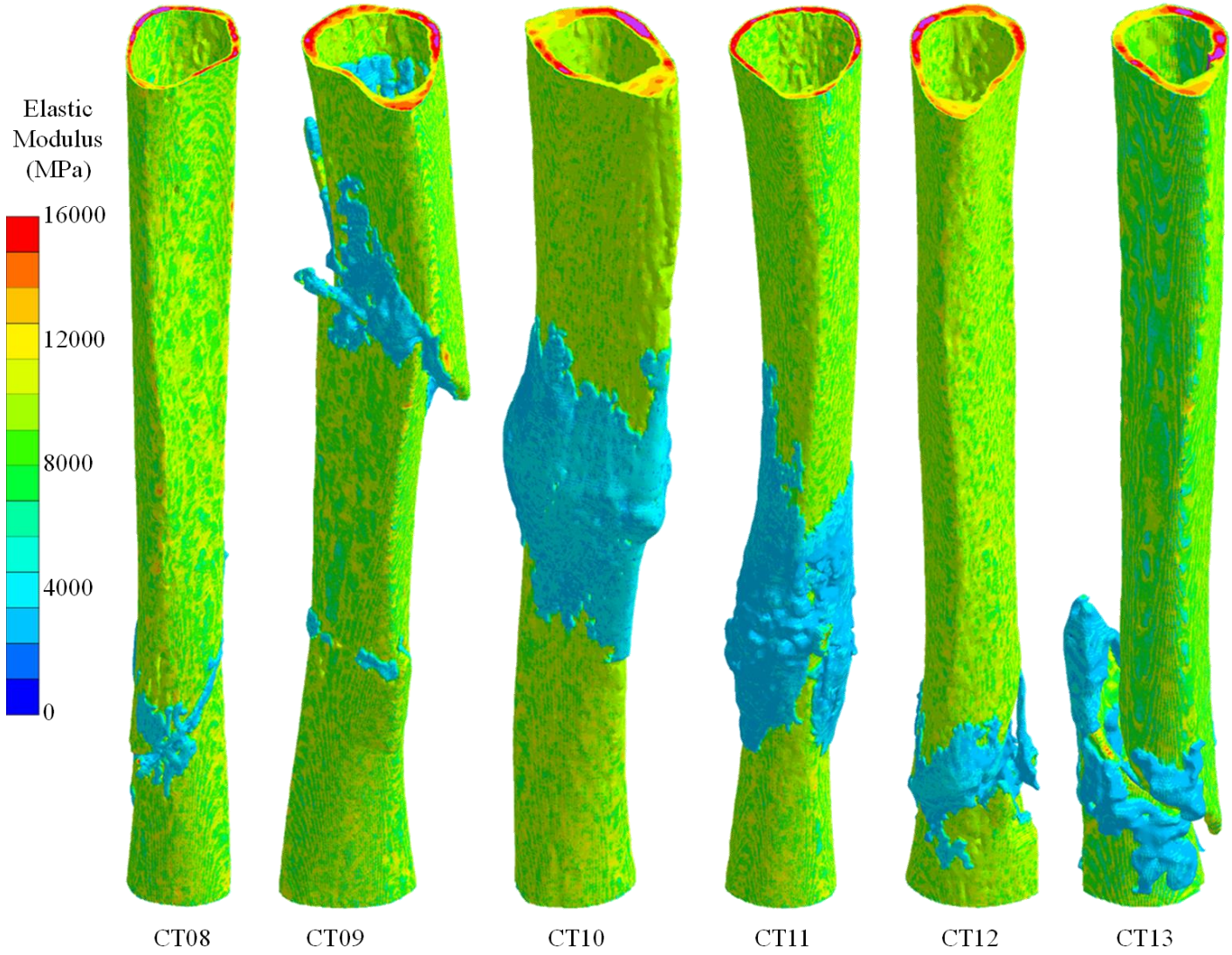

Figure 6: Elastic Moduli Contour Plots for CT08-CT13

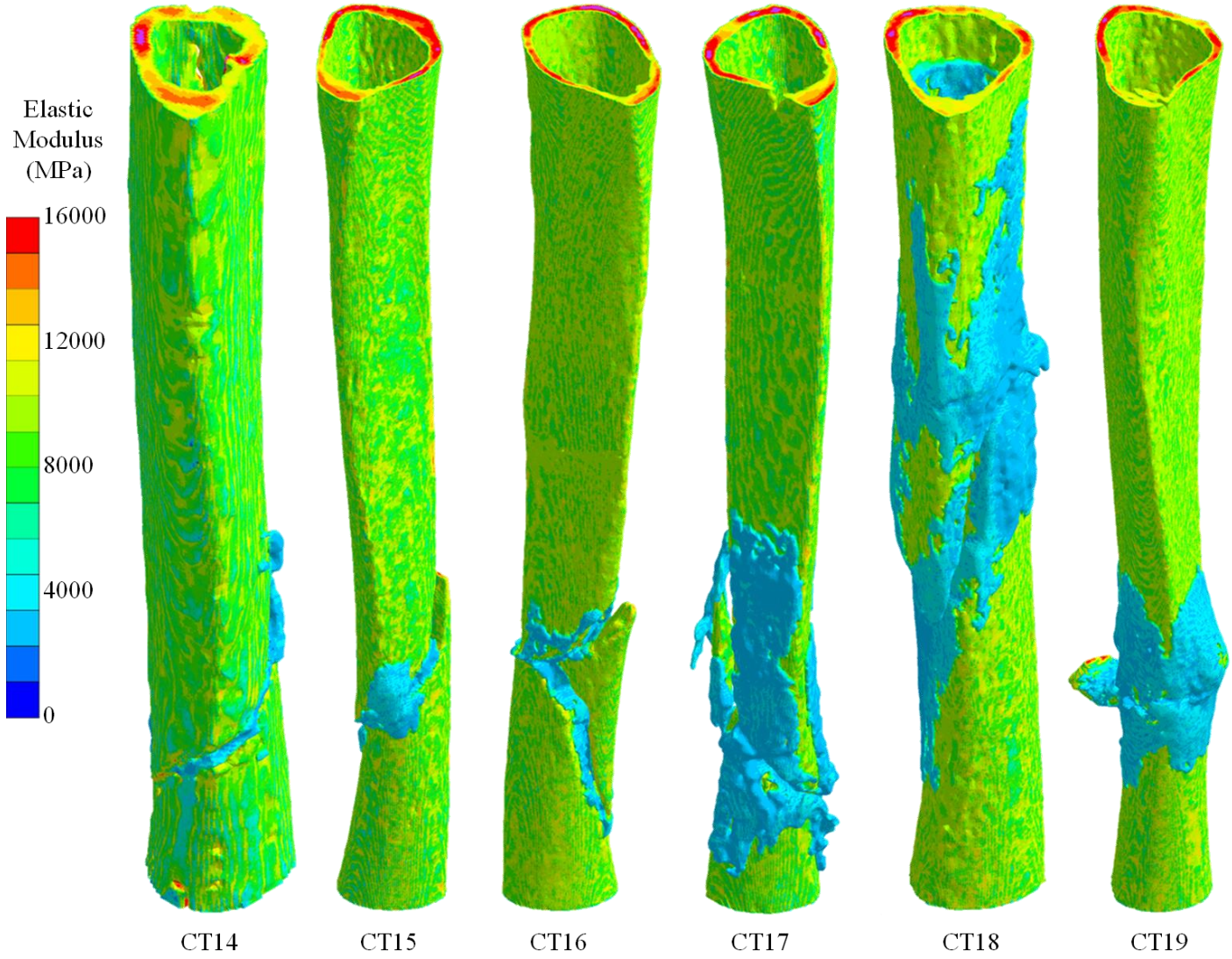

Figure 7: Elastic Moduli Contour Plots for CT14-CT19

E. Reconstructed Finite Element Models

Within the group of individuals recruited for this study, considerable variations were observed in stature, bone quality, and cortical bone thickness. All of these physical and mechanical differences fundamentally influence the expected torsional stiffness of the pre-injured bone and confound the comparison between individuals at the 12-week time point. To minimize the between-individuals differences that were unrelated to the injury pattern and healing response, each individual's cortical bone fragments were digitally reconstructed to form a virtual intact model. The same DICOM image sets were imported into the Mimics, which segmented strictly old cortical bone into surface models. We then reconstructed the segments into an equivalent intact tibia. Reconstruction of the intact anatomy was straightforward and unambiguous for simple fractures (e.g. OTA/AO type A) and more challenging for multi-fragmentary cases (e.g. OTA/AO type B and C injuries). A wrapping function united the bone fragments into a single surface and a volumetric mesh was calculated, but was completed with a focus on restoring the functional mechanical axis of the bone. After wrapping, appropriate 3D anatomical alignment of each reconstructed tibia was confirmed visually. For the reconstructed models, 3-D fragment realignment eliminates the option to define voxel-derived elementwise mechanical properties, so a reference homogeneous Young's modulus for each cortical segment was calculated using the median HU value in that segment and the same scaling rule as before.

F. Virtual Torsion Testing

In preclinical models of fracture healing, torsional rigidity is a commonly used rotational stiffness parameter that results from a single post-mortem mechanical test. Torsional stiffness relative to intact paired controls is generally used as a summary index of healing progress because these tests are destructive, so only one measurement can be performed. Although some investigators have chosen to report bending stiffness as a summary structural parameter in computational modeling studies, the bending stiffness is highly affected by the rotational orientation of the tibia during testing, whereas the torsional stiffness is not [18]. For this investigation, we chose to calculate virtual torsional rigidity (VTR) to mimic *in vitro* torsional tests. VTR is defined as the moment reaction from the applied loading (M) multiplied by the length of the test segment (L) divided by the resultant angle of twist (ϕ): $VTR = ML/\phi$ [N-m^2/°]. For the virtual test, the angle of twist was applied such that the proximal surface was rotated about the mechanical axis of the tibia with the most-distal surface rigidly fixed, as would be the case in physical testing. The moment reaction was the calculated moment induced on the distal face by the applied angle of twist.

All structural simulations were carried out in ANSYS 17.2. Finite element meshes created in Mimics were imported into ANSYS with elementwise material properties. Boundary conditions of rigid fixation on the distal end and 1 degree of rotation on the proximal end were then applied. A sensitivity study was conducted on the linearity of the model showing less than 1% differences in VTR with up to 10 degrees of rotation. The static structural model was then solved and moment reactions reported to allow calculation

of VTR. This process was repeated for both the injured limb models and the reconstructed intact models. VTR of each fractured model was then normalized to that individual's own reconstructed models to help remove individual anatomical variation between patients.

G. Statistical Analysis

Descriptive statistics were generated using Microsoft Excel (2016) and MATLAB (R2016a, The MathWorks, Inc., Natick, Massachusetts). Unless otherwise indicated, values are reported as medians and interquartile ranges. Additional statistical analysis was conducted in SPSS (25.0)(IBM Corp., Armonk, NY). Correlations between various morphometric and structural parameters were assessed using Pearson's correlation coefficient to correlate the different parameters.

III. Results

A. Morphometric data

For each individual, the distribution of radiodensity in both the callus and cortical bone was assessed. These distributions were all non-normally distributed by the Kolmogorov-Smirnov test (all $p > 0.05$), so the median Hounsfield Unit was reported for each model in each tissue zone (see Table 3). Comparing across all individuals included in the study, the median callus density was 778 (729.5 – 805.5) HU, see also Figure 8. Each model's segmented callus volume was also recorded. The median callus volume across the 19 fracture models was 9.08 (7.19 – 14.38) cm^3, see also Figure 9. The median number of elements in each FE model was 2,608,909 (2,169,891 – 2,872,787) tetrahedral-4 elements. The median RUST score assigned by the attending orthopaedic surgeon based on 12-week X-rays was 10.5 (8.25 – 12), see also Figure 10.

CT Case Number	Median Callus Density		Callus Volume	Median Bone Density		Number of Elements	Working Length	12 Week RUST Scores	VTR
[-]	[HU]	[Q1 - Q3]	[cm^3]	[HU]	[Q1 - Q3]	[-]	[mm]	[-]	[N-m^2/°]
CT01	806	(621 - 1029)	7.57	2121	(1950 - 2270)	1.74E+06	201.26	12	1.51
CT02	716	(525 - 994)	14.95	2060	(1865 - 2210)	3.14E+06	265.63	8	3.70
CT03	752	(552 - 1033)	7.78	2040	(1852 - 2188)	2.89E+06	258.76	8	1.71
CT04	702	(553 - 946)	5.30	2065	(1884 - 2206)	2.59E+06	258.13	11	2.46
CT05	860	(613 - 1108)	11.70	1739	(1614 - 1921)	1.71E+06	178.14	12	1.90
CT06	743	(540 - 1069)	6.68	1927	(1756 - 2065)	2.11E+06	223.76	11	1.07
CT07	787	(583 - 1057)	9.08	1942	(1791 - 2084)	3.20E+06	276.26	12	4.13
CT08	778	(582 - 1016)	8.53	2053	(1844 - 2236)	2.62E+06	255.63	5	1.74
CT09	768	(561 -1061)	32.20	1987	(1786 - 2122)	3.18E+06	245.01	11	2.90
CT10	926	(682 - 1166)	14.75	1919	(1725 - 2083)	1.82E+06	196.27	12	2.04
CT11	795	(597 - 1038)	25.10	2017	(1802 - 2196)	2.61E+06	249.38	12	2.68
CT12	708	(532 - 1010)	11.94	1958	(1791 - 2117)	2.71E+06	241.26	9	2.78
CT13	667	(524 - 895)	6.81	1975	(1798 - 2124)	2.23E+06	227.51	4	0.17
CT14	799	(597.5 - 1057)	2.57	1910	(1748 - 2049)	1.68E+06	178.13	9	1.98
CT15	805	(585 - 1064)	4.28	2070	(1905 - 2187)	2.69E+06	259.39	5	2.42
CT16	764	(580 - 1002)	9.07	2104	(1922 - 2220)	2.96E+06	266.26	10	2.67
CT17	693	(526 - 979)	12.66	1933	(1778 - 2079)	2.56E+06	237.51	12	1.74
CT18	959	(643 - 1238)	28.73	1931	(1572 - 1972)	2.28E+06	208.14	11*	1.64
CT19	832	(605 - 1109)	14.02	1924	(1757 - 2071)	2.85E+06	263.14	10	2.92

Table 3: Morphometric properties of the 19 patient models. Callus and bone density were calculated from Hounsfield Units of original CT scan data. Callus volume was calculated from the surface model created in Mimics Innovation Suite. Number of elements is the number of tetrahedral-4 elements in each FE model. Length is the distance from distal to proximal surface. VTR is the virtual torsional rigidity of the fractured model. *12 Weeks RUST Score from CT scan.

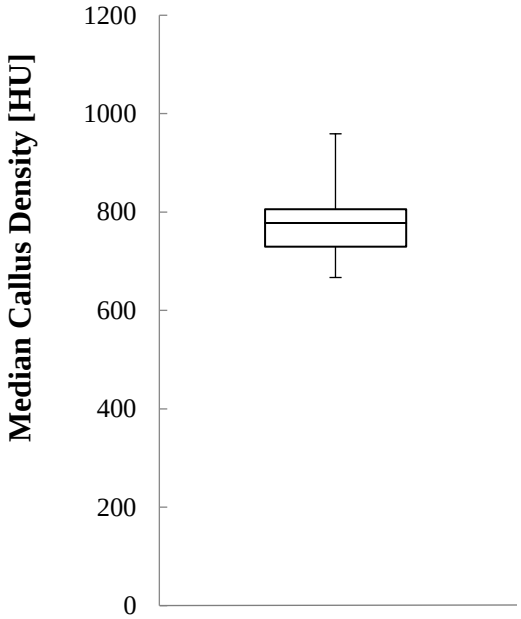

Figure 8: Box plot of the callus density distribution across the 19 patient models. Median (Q1 – Q3): 778 (730 – 806) HU.

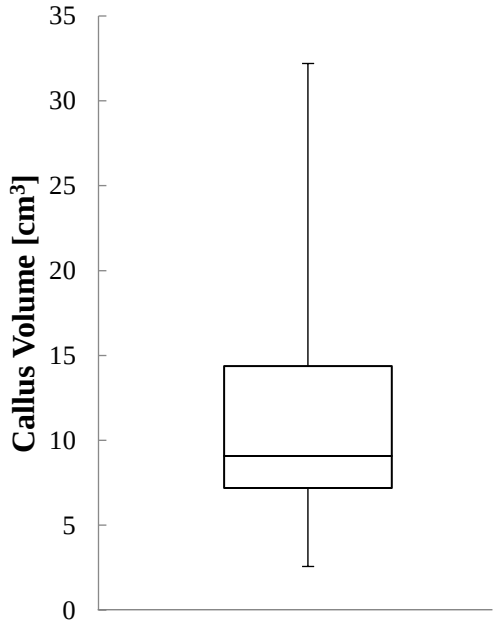

Fig 9: Box plot of the callus volume distribution across the 19 patient models. Median (Q1 – Q3): 9081 (7186 – 14385) mm³.

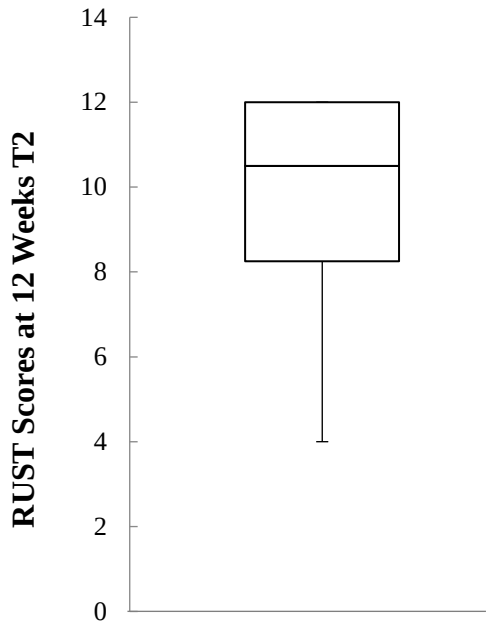

Figure 10: Box plot of the distribution of RUST scores at 12 weeks. Median (Q1 - Q3): 11 (8.3 - 12)

B. Structural data: VTR

Virtual torsional rigidity was calculated for each fracture model and had a median value of 2.04 (1.73 – 2.73) N-m^2/°. Additionally, the VTR was calculated for each reconstructed model, yielding a median value of 2.53 (2.14 – 3.24) N-m^2/°. Previously published values for the torsional rigidity of intact cadaver tibia indicate an expected mean value 2.42 ± 0.80 N-m^2/° [23], indicating that model results were within the expected physiological range. The fractured models were normalized to their own reconstructed model to calculate a normalized VTR value representing how each patient's healing has progressed. The normalized VTR was found to be 0.86 (0.74 – 0.96) [-]. This distribution can be seen in Figure 11.

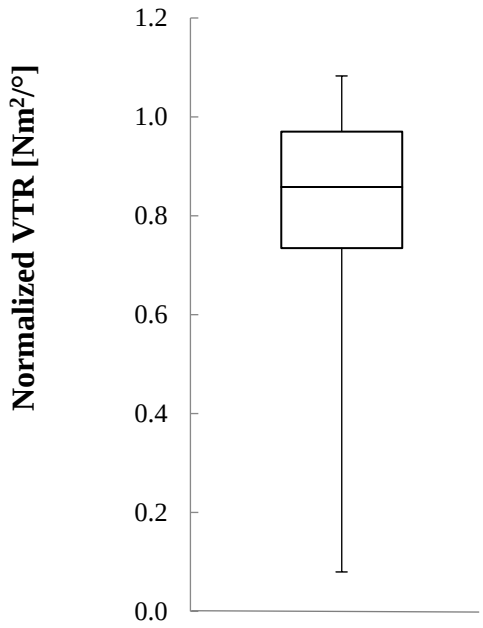

Figure 11: Box plot of the normalized VTR distribution across the 19 patient models. Median (Q1 – Q3): 0.86 (0.735 – 0.959).

C. Statistical Correlations

Statistical correlation analysis was used to assess whether clinically relevant observable relationships may exist between any of the morphometric and structural healing measures. For this analysis, five measures were considered: callus volume, callus density, RUST scores, virtual torsional rigidity (VTR) of the fractured tibia, and VTR of the reconstructed intact bone models. These correlations were designed to address clinically significant questions arising in the subjective interpretation of callus on typical plain film X-rays. First, we considered, "Is a larger quantity of visible callus indicative of better healing?" as represented by the relationship between callus volume and VTR of the fracture bone (see Figure 12). This correlation was weak and non-significant, indicating that a larger quantity of external callus is not necessarily predictive of a stiffer bone.

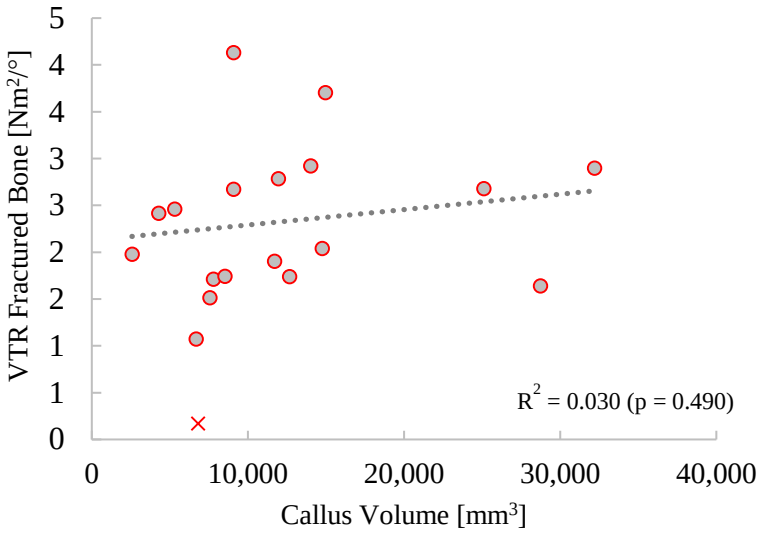

Figure 12: Scatter plot of callus volume vs. VTR of reconstructed bone. Outlier plotted with an "X".

Next, we considered, “Is denser-looking callus indicative of better healing?” as represented by the relationship between callus density and VTR of the fractured bone (see Figure 13). This correlation was also weak and non-significant, indicating that a denser-looking external callus is not necessarily predictive of a stiffer bone.

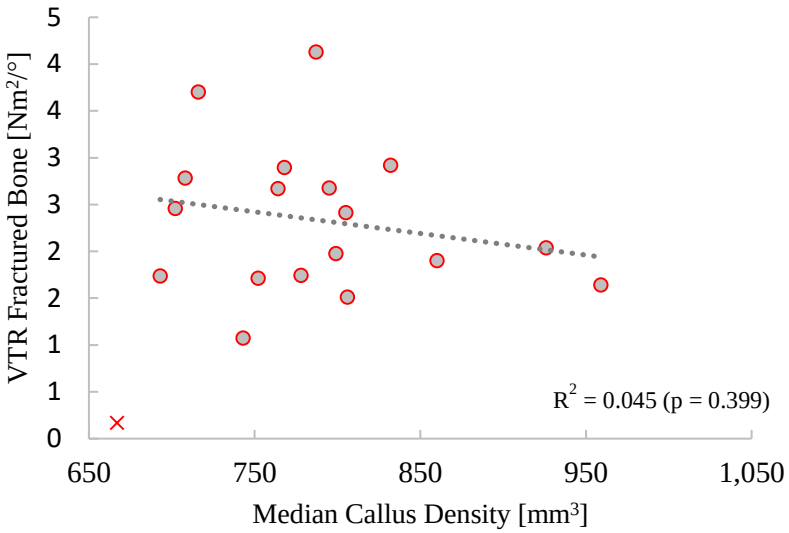

Figure 13: Scatter plot of callus density vs. VTR of reconstructed bone. Outlier plotted with an “X”.

We addressed the orthopaedic surgeon's assessment of the healing progress of the bone. This is represented by the relationship between normalized VTR and the clinical RUST scores at 12 weeks. There was a moderate correlation ($R^2 = 0.311$) that was significant ($p < 0.05$), showing that the subjective visual assessment of an experienced surgeon can provide information on the structural integrity of the fracture. (Figure 14)

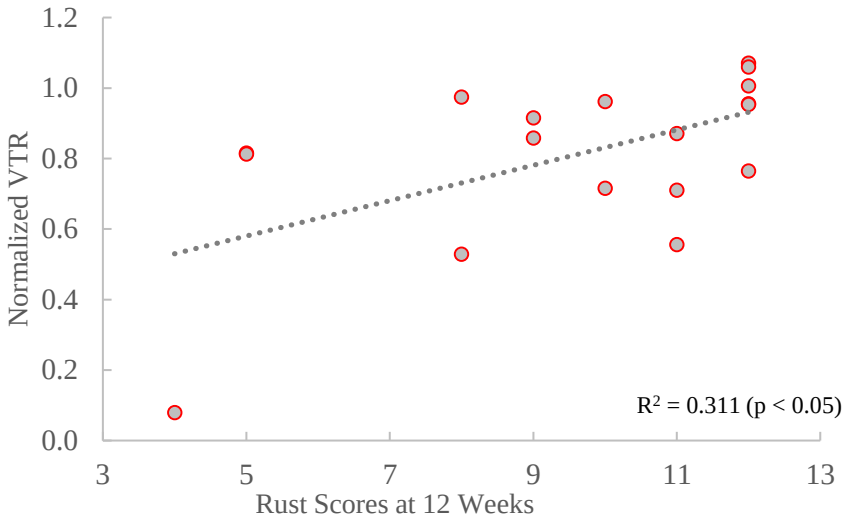

Figure 14: Scatter plot of normalized VTR vs. RUST scores.

Finally, we considered, “Does the patient’s anatomy (stature and cortical bone thickness) influence the stiffness of the partially healed bone?” as represented by the relationship between fractured VTR and reconstructed VTR. This correlation was strong ($R^2 = 0.699$) and significant ($p < 0.001$). Collinearity between fractured VTR and reconstructed VTR was confirmed with a multi-variate linear regression on four variables (callus volume, callus density, fracture VTR, and reconstructed VTR). This indicates that the torsional rigidity of the partially healed bone is significantly related to that of the uninjured limb.

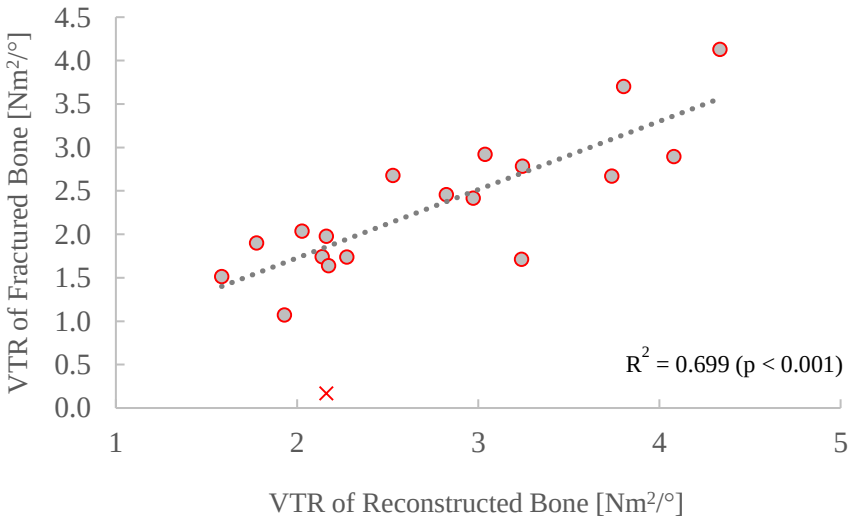

Figure 15: Scatter plot of VTR of fractured limb vs. VTR of reconstructed bone. Outlier plotted with an “X”.

IV. Discussion

Traditional radiographic assessment of fracture healing has relied on human subjective interpretation of the quantity and quality of visible callus on X-rays, with the assumption that more denser-looking callus indicates a stiffer healing zone. Qualitatively, this may be true, but the quantitative data presented in this work shows that observations about callus size or density do not necessarily independently predict the structural integrity of the partially healed bone. In this study, we found that morphometric measures (e.g. callus volume and density) have a weak and non-significant correlation with torsional rigidity. This is because both the geometry and material properties influence how the loading through the limb is distributed. Simply measuring the connectivity and volume of callus without including material mechanics does not accurately represent the complex structure of the healing zone. In some cases, these morphometric parameters can even misguide the determination of the healing progress. For example, some models in this case series had a large volume of low density callus and therefore had high VTR. Conversely, some cases with low callus volume had much higher density, leading again to high VTR. These results suggest that neither callus morphometry nor callus material composition alone is sufficient to predict the structural progress of healing. Clinically, RUST scores are used to evaluate material and shape. While RUST scores are moderately predictive of torsional rigidity, some models had large differences between RUST scores and VTR due to a small amount of stronger callus. The virtual mechanical test method we have develop combines these two factures – material and shape – to create a simple and intuitive measure of the structural progress toward full recovery.

Dealing with individual anatomic variations is a notable challenge in biomechanical studies. In this case series, the coefficient of variation for VTR of the reconstructed intact limbs was 29.2%, illustrating the significant anatomical differences observed between patients within this group. These variations are important to understand because they may confound interpretation of healing progress in the injured limb. This concern is supported by the fact that we observed a strong and statistically significant correlation between VTR of the fractured model and the reconstructed models, with a Pearson's correlation coefficient (R^2) of 0.699 ($p < 0.001$). To minimize the effect of these variations, VTR of each patient's fracture was normalized to their own reconstructed model. This normalization allows a comparison of all 19 subjects to their own pre-fractured bone and insight into their individual healing process. The coefficient of variation of the normalized VTR for all 19 cases in this series was 28.07%. Although the normalized VTR has similar variability to the non-normalized VTR, the process of referencing each model to its own intact bone ensures that the variations observed are related to the fracture pattern and healing response, rather than the individual anatomical variations.

The central premise of this study was that a virtual mechanical analysis technique may be useful for characterizing the typical fracture healing response of a cohort of similarly managed cases. Figure 11 shows that in our cohort, more than 75% of patients (first quartile and above) achieved a torsional rigidity equivalent to at least 75% of their intact limb at 12 weeks. In this cohort, there was only one fracture model that was an outlier using Tukey's inner fence criteria, with a normalized VTR of 8%. This may be indicative of a possible non-union, although non-unions are not routinely diagnosed until at least 6-9

months post-op [9] . Two other fractures in this cohort fell well below the 75% benchmark with normalized VTRs of 53% and 56%. These cases were not statistically outliers but may indicate that the patients need attention and monitoring for a possible delayed union. Based on these findings, we propose that a "75/75 rule" (75% of patients will achieve at least 75% of their own intact bone rigidity) at 12 weeks may be an intuitive and actionable decision-making guide for earlier identification of patients who are experiencing compromised healing and may require intervention to treat or prevent a non-union.

One final advantage of the VTR method we have proposed is that the minimization of individual anatomical variations makes the resulting outcome parameter statistically powerful and could allow for smaller recruitment targets for clinical studies. For example, to detect a difference of 20% between two hypothetical treatment groups at 80% power and a significance level of 0.05, outcomes assessments based on callus volume would require sample sizes 163 patients per group. By comparison, a sample size of only 31 patients per group would be required to detect the same difference in normalized VTR. This sample size is similar to the result based on using RUST scores (N = 32), but the virtual structural analysis has the advantage of being truly objective and fully quantitative without a ceiling effect (i.e. max RUST score of 12) and no treatment bias. By these measures, VTR allows new and powerful insight into the biomechanical tissue-adaptation response to osteosynthesis and offers and intuitive outcome measure that could detect differences between patient groups with much smaller recruitment targets than are currently the norm. Studies that investigate topics such as patient risk factors, surgical

implant selection, surgical technique, or post-operative rehabilitation can greatly benefit from this technique.

This investigation has a few noteworthy limitations. First, the torsional rigidity of human clinical fractured tibiae cannot be measured by any direct physical means to validate the VTR of the 12 weeks scans. However, the calculated torsional rigidities of the reconstructed intact limbs are within the range of previously reported values for intact cadaver tibiae [23]. Ovine models are the next logical step to develop a scaling function between density and elastic moduli across the callus.

Another limiting factor in patient-specific models with element-wise density-based mechanical properties is the limited availability of validated Young's modulus scaling laws for the tissues that are relevant for fracture healing. While there are many distinct models to predict elastic moduli of cortical and trabecular bone regions based on density measurements from image analyses, there is little agreement between these models and understandably little data on numerical models for new bone growth in callus region [24]. For our study, the same scaling power law scaling was applied for all patients using the equation $E = HU \times 0.00704$ GPa. (reported as $E = 70.4 \times 10^5 \times HU$) [22]. This scaling law is not necessarily the only appropriate or best option, but by applying it consistently across all patients as part of controlled model-generation workflow, we have established a technique that has utility as a comparative tool for assessing between- and within-group variations in clinical orthopaedic trauma research.

V. Conclusions

Image-based structural mechanics modeling from low-dose CT is a robust, repeatable, objective, quantitative, and powerful approach to assessing fracture healing in clinical orthopaedic trauma research. Using the method described above, we were able to quantitatively access the structural progress of fracture healing compared to each patient's own intact bone. The results provide insights into fracture healing that are not possible with the suite of qualitative and semi-quantitative observational measures typically used in clinical studies. These semi-quantitative measures, such as volume, can even lead to incorrect conclusions about a patient's healing. The virtual torsional rigidity technique also shows much lower variability than traditional morphometric data and may enable hypothesis testing in orthopaedic trauma research with much smaller recruitment targets.

Bibliography

[1] H. L. Dailey, K. Wu, P.-S. Wu, M. McQueen, and C. Court-Brown, "Tibial fracture nonunion and time to healing following reamed intramedullary nailing: Risk factors based on a single-centre review of 1003 patients," *J. Orthop. Trauma*.

[2] D. Höntzsch *et al.*, "Evaluation of the effectiveness of the angular stable locking system in patients with distal tibial fractures treated with intramedullary nailing: A multicenter randomized controlled trial," *J. Bone Jt. Surg. - Am. Vol.*, 2014.

[3] M. Bhandari *et al.*, "Randomized trial of reamed and unreamed intramedullary nailing of tibial shaft fractures," *J. Bone Jt. Surg. - Ser. A*, vol. 90, no. 12, pp. 2567–2578, 2008.

[4] M. Bhandari, G. H. Guyatt, M. F. Swiontkowski, I. Paul Tornetta, S. Sprague, and E. H. Schemitsch, "A Lack of Consensus in the Assessment of Fracture Healing Among Orthopaedic Surgeons," vol. 16, no. 8, pp. 562–566, 2002.

[5] D. B. Whelan *et al.*, "Development of the radiographic union score for tibial fractures for the assessment of tibial fracture healing after intramedullary fixation," *J. Trauma - Inj. Infect. Crit. Care*, vol. 68, no. 3, pp. 629–632, 2010.

[6] J. M. Leow, N. D. Clement, T. Tawonsawatruk, C. J. Simpson, and A. H. R. W. Simpson, "The radiographic union scale in tibial (RUST) fractures: Reliability of the outcome measure at an independent centre," *Bone Jt. Res.*, vol. 5, no. 4, pp. 116–121, 2016.

[7] J. Litrenta *et al.*, "Determination of Radiographic Healing: An Assessment of Consistency Using RUST and Modified RUST in Metadiaphyseal Fractures," *J. Orthop. Trauma*, vol. 29, no. 11, pp. 516–520, 2015.

[8] R. C. Castillo *et al.*, "Improving pain management and long-term outcomes following high-energy orthopaedic trauma (pain study)," *J. Orthop. Trauma*, vol. 31, no. 4, pp. S71–S77, 2017.

[9] J. A. Bishop, A. A. Palanca, M. J. Bellino, and D. W. Lowenberg, "Assessment of compromised fracture healing," *J. Am. Acad. Orthop. Surg.*, vol. 20, no. 5, pp. 273–282, 2012.

[10] K. O'Halloran *et al.*, "Will My Tibial Fracture Heal? Predicting Nonunion at the Time of Definitive Fixation Based on Commonly Available Variables," *Clin. Orthop. Relat. Res.*, vol. 474, no. 6, pp. 1385–1395, 2016.

[11] A. H. Van Houten, P. J. C. Heesterbeek, R. J. Van Heerwaarden, T. G. Van Tienen, and A. B. Wymenga, "Medial open wedge high tibial osteotomy: Can delayed or nonunion be predicted?," *Clin. Orthop. Relat. Res.*, vol. 472, no. 4, pp. 1217–1223, 2014.

[12] S. V. N. Jaecques *et al.*, "Individualised, micro CT-based finite element modelling as a tool for biomechanical analysis related to tissue engineering of bone," *Biomaterials*, vol. 25, no. 9, pp. 1683–1696, 2004.

[13] E. F. Morgan *et al.*, "Micro-computed tomography assessment of fracture healing: Relationships among callus structure, composition, and mechanical function," *Bone*, vol. 44, no. 2, pp. 335–344, 2009.

[14] G. Chen *et al.*, "A new approach for assigning bone material properties from CT

images into finite element models," *J. Biomech.*, vol. 43, no. 5, pp. 1011–1015, 2010.
[15] S. J. Shefelbine *et al.*, "Prediction of fracture callus mechanical properties using micro-CT images and voxel-based finite element analysis," *Bone*, vol. 36, no. 3, pp. 480–488, 2005.
[16] J. Gao, H. Gong, X. Huang, J. Fang, D. Zhu, and Y. Fan, "Relationship between microstructure, material distribution, and mechanical properties of sheep tibia during fracture healing process," *Int. J. Med. Sci.*, vol. 10, no. 11, pp. 1560–1569, 2013.
[17] S. M. Porter, H. L. Dailey, K. A. Hollar, K. Klein, J. A. Harty, and T. J. Lujan, "Automated measurement of fracture callus in radiographs using portable software," *J. Orthop. Res.*, 2016.
[18] P. Augat *et al.*, "Interfragmentary movement in diaphyseal tibia fractures fixed with locked intramedullary nails," *J. Orthop. Trauma*, vol. 22, no. 1, pp. 30–36, 2008.
[19] G. Li, X. Liu, C. T. Dodge, C. T. Jensen, and X. J. Rong, "A noise power spectrum study of a new model-based iterative reconstruction system : Veo 3 . 0," *J. Appl. Clnical Med. Phys.*, vol. 17, no. 5, pp. 428–439, 2016.
[20] K. Li, J. Tang, and G.-H. Chen, "Statistical model based iterative reconstruction (MBIR) in clinical CT systems: Experimental assessment of noise performance," *Med. Phys.*, vol. 41, no. 4, p. 41906, 2014.
[21] C. Ament and E. Hofer, "A fuzzy logic model of fracture healing," *J. Biomech.*, vol. 33, no. 8, pp. 961–968, 2000.
[22] S. M. Snyder and E. Schneider, "Estimation of mechanical properties of cortical bone by computed tomography," *J. Orthop. Res.*, vol. 9, no. 3, pp. 422–431, 1991.
[23] A. D. Heiner, "Structural properties of fourth-generation composite femurs and tibias," *J. Biomech.*, vol. 41, no. 15, pp. 3282–3284, 2008.
[24] M. Tuncer, U. N. Hansen, and A. A. Amis, "Prediction of structural failure of tibial bone models under physiological loads: Effect of CT density-modulus relationships," *Med. Eng. Phys.*, vol. 36, no. 8, pp. 991–997, 2014.

Vita:

Peter Schwarzenberg was born in Kingwood, West Virginia, on June 28, 1994. He enrolled at Lehigh University in 2012 and completed his Bachelor's Degree in Mechanical Engineering in 2016. As an undergraduate, Peter won the Andrew Wilson Knecht III Memorial Award as the senior who has exhibited the greatest potential for applying technical training to practical application. After his undergraduate studies, Peter remained at Lehigh University for graduate school.